WIND GENERATOR DRIVETRAIN PERFORMANCE AND COMPARISON OF PM FLUX SWITCHING MACHINES

Udochukwu B. AKURU
Tshwane University of Technology
Department of Electrical Engineering, Tshwane University of Technology, Pretoria 0183, South Africa
AkuruUB@tut.ac.za

Abstract: *This study is undertaken to highlight the competitive optimal performance of permanent magnet flux switching machines (PM–FSMs) in different wind generator drivetrains—low–speed (LS), medium–speed (MS) and high–speed (HS). The three–phase 12–stator slots/10–rotor teeth PM–FSM is selected for the study, for small–scale power applications. The design and optimisation is performed using a 2–D finite element analyses (FEA) tool. Thereafter, important features of the different wind generator drivetrains are evaluated and compared, especially in terms of cost of energy (CoE) versus performance. In the end, the study barely stops short of representing the MS as the best among the three drivetrains; however, it is clearly a preferred solution due to trade–offs in torque density and cost of generator.*

Key words: *cost of energy (CoE), design optimisation, finite element analyses (FEA), permanent magnet flux switching machine (PM-FSM), wind generator drivetrain.*

1. Nomenclature

α	current angle [deg.].
Δ	load angle [deg.].
V_s	phase voltage [V].
E_q	no–load generated voltage [V].
I_s	phase current [A].
λ_d & λ_q	d– and q–axes flux linkages [Wb.].
λ_M	no–load flux linkage [Wb].
L_d & L_q	d– and q–axes inductances [H].
I_d & I_q	d– and q–axes phase currents [A].
Π	a variable to represent phase vector quantities like flux linkages or currents.
d, q, & 0	Park's transformation variables.
a, b, & c	three–phase variables.
θ	Park's transformation angle [rad.].
V_d & V_q	d– and q–axes phase voltages [V].
ω_e	electrical speed [rad/s].
R_s	total phase resistance [Ω].
q	number of phase coils in series connection.
N_{ph}	turns number per coil for the phase windings.
ρ_{Cu}	resistivity of copper wire [Ω.m].
l_{st}	axial or stack length [m].
l_{ϑ}	distance of the phase end–winding from lamination [m].
A_{ph}	area of the phase wire [m^2].
N_r	PM–FSM rotor teeth number.
τ_e	electromagnetic torque [Nm].
κ_δ	torque ripple [%].
$\tau_{e(\max)}$ & $\tau_{e(\min)}$	upper and lower peaks of τ_e [Nm].
C_m, σ and β	Steinmetz coefficients for core loss estimation.
$\dot{B}_k$	peak flux density measured in k iron core part [Wb].
M_k	mass of k iron core part [kg].
N	number of iron core parts.
f_e	frequency [Hz].
$\mathcal{P}_{\text{out}}$	real power [W].
Q	reactive power [W].
P_{Cu}	copper loss [W].
P_{Core}	core losses [W].
η	efficiency [%].
PF	power factor.
M_{PM}	mass of the PM [kg].
M_A	total active mass [kg].
M_{FeS}	mass of the stator iron [kg].
M_{FeR}	rotor iron mass [kg].
M_{Cu}	copper mass of phase windings [kg].
$x^{(L)}$ and $x^{(U)}$	lower and upper boundary limits of designated design variable.
Λ_0	split ratio.
κ_L	aspect ratio.
J	phase current density [A/mm^2].

2. Introduction

In recent times, wind turbine manufacturers have increasingly shifted their focus to geared medium–speed (MS) drivetrains for wind turbine systems because of some challenges encountered in low–speed (LS) and high–speed (HS) systems, such as higher manufacturing and maintenance costs [1]. In addition, the impetus to tap the vast wind energy potential which exists both onshore and offshore is increasing because it guarantees a good return on investment (ROI) for wind turbines that are designed at industrial–scale power levels. Hence, geared MS systems, as shown in Fig. 1, offer a reliable compromise for such industrial–scale wind turbines, in terms of the gearbox and generator sizes. Note also, the presence of the solid state converters (SSCs) as critical components of the proposed drivetrain architecture. Recent trends which show the benefits of geared MS drivetrains over LS and HS drivetrains have already been addressed in [2], based on the drivetrain performance comparison of PMSGs.

Also, studies in [3, 4] regarding MS doubly-fed induction generators (DFIGs) and permanent magnet

synchronous generators (PMSGs), respectively, both portrayed lowest cost of energy (CoE) compared to LS and HS systems. Consequently, to capitalise on these latent benefits, there is need to do further research to highlight important qualities of newer concept of wind generators designed for geared MS drivetrains, while comparing for highest CoE. Such studies appear not to have been documented for permanent magnet flux switching machines (PM–FSMs)—typically, a non–conventional machine—gaining wide usage because of its stator–mounted (and brushless) qualities [5, 6].

In this paper, an attempt is made to compare the optimum design performance of the very popular 12–stator slots/10–rotor teeth (12/10) radial–flux PM–FSM topology in the different wind generator drivetrains, for the first time. To achieve this, 2–D static finite element analyses (FEA) method is employed for both the optimisation and the performance evaluation. Eventually, the design feasibility is established by 3–D FEA process applied to a benchmark design.

3. Electromagnetic modelling of the PM–FSM

The design optimisation and performance evaluation process is to be undertaken by means of an in–house Python script–based non–linear 2–D static FEA program, called SEMFEM [7]. But before the design optimisation process, it is important to set forth, for the PM–FSM, the steady–state d– and q–axes (dq) equations which will be implemented in the FEA package. This way, the speed of the design optimisation process is hopefully enhanced.

Consequently, the steady–state dq equivalent circuits and phase diagram, in generator mode, are shown in Fig. 2. Note that, $V_s > E_q$ and that I_s lags V_s as implied in Fig. 2. To associate the meaning of the variable terms, a list of nomenclature has been provided at the beginning of the paper. Based on the evaluation of the 2–D FEA model, the dq axes flux linkages, from which other machine characteristics are devised, are given as

$$\lambda_d = \lambda_M + L_d I_d, \tag{1}$$
$$\lambda_q = L_q I_q, \tag{2}$$

where all the parameters have been defined accordingly in section I.

The expressions in (1) and (2) are used to facilitate the determination of the dq inductances. In reality, the dq flux linkages are fundamental output variables resulting from the SEMFEM technique which prescribes as input variables, the field excitation source and phase currents of a proposed electrical machine design. To this end, the 2–D FEA program evaluates the dq quantities mainly from their fundamental phase quantities by using Park's dq transformation equation expressed as

$$\begin{bmatrix} \Pi_d \\ \Pi_q \\ \Pi_0 \end{bmatrix} = \frac{2}{3}\begin{bmatrix} \cos\theta & \cos\left(\theta + \frac{2\pi}{3}\right) & \cos\left(\theta - \frac{2\pi}{3}\right) \\ \sin\theta & \sin\left(\theta + \frac{2\pi}{3}\right) & \sin\left(\theta - \frac{2\pi}{3}\right) \\ \frac{1}{2} & \frac{1}{2} & \frac{1}{2} \end{bmatrix}\begin{bmatrix} \Pi_a \\ \Pi_b \\ \Pi_c \end{bmatrix}, \tag{3}$$

where all the parameters have been defined accordingly in section I.

The dq axes voltages are evaluated as

$$V_d = \omega_e L_q I_q - R_s I_d, \tag{4}$$
$$V_q = \omega_e \lambda_M - \omega_e L_d I_d - R_s I_q, \tag{5}$$

where all the parameters have been defined accordingly in section I.

The phase resistance is given as

$$R_s = 2qN_{ph}^2 \rho_{Cu} \frac{l_{st}+l_e}{A_{ph}}, \tag{6}$$

where all the parameters have been defined accordingly in section I.

The magnitudes of the phase output voltage and current are calculated as

$$V_s = \sqrt{V_d^2 + V_q^2}, \quad I_s = \sqrt{I_d^2 + I_q^2}, \tag{7}$$

where all the parameters have been defined accordingly in section I.

The torque and torque ripple are given as

$$\tau_e = \frac{3}{2} N_r \left(I_q \lambda_M + \left(L_d - L_q\right) I_d I_q\right), \tag{8}$$
$$\kappa_\delta = \frac{\tau_{e(\max)} - \tau_{e(\min)}}{\tau_e}, \tag{9}$$

where all the parameters have been defined accordingly in section I.

The real and reactive power, total copper and core losses are given as follows:

$$\mathcal{P}_{\text{out}} = \frac{3}{2}\left(V_d I_d + V_q I_q\right), \tag{10}$$
$$\mathrm{Q} = \frac{3}{2}\left(V_q I_d - V_d I_q\right), \tag{11}$$
$$P_{Cu} = \frac{3}{2}\left(I_d^2 + I_q^2\right) R_s, \tag{12}$$
$$P_{Core} = C_m f_e^\beta \sum_{k=1}^{N} \dot{B}_k^\sigma M_k. \tag{13}$$

In this study, non–oriented fully processed M400–50A gauge magnetic steel grade with mass density 7600 kg/m^3 is the preferred core sheets from which the Steinmetz coefficients (C_m, σ and β) are determined from the core loss-frequency curves.

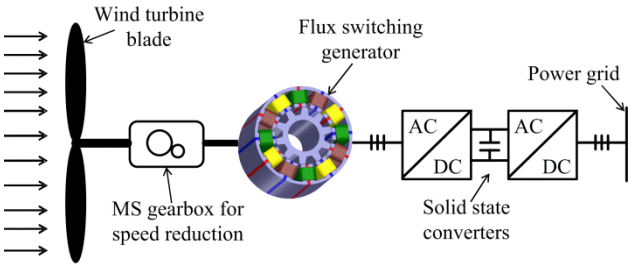

Fig. 1. The proposed wind generator drivetrain.

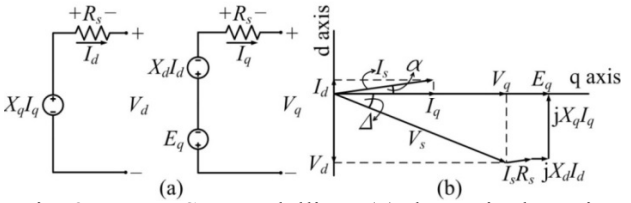

Fig. 2. PM–FSM modelling: (a) dq equivalent circuits, (b) phasor diagram.

Lastly, the efficiency and power factor is given as

$$\eta = \frac{\mathcal{P}_{\text{out}}}{\mathcal{P}_{\text{out}}+P_{Cu}+P_{Core}}, \tag{15}$$

$$\text{PF} = \cos\left(\tan^{-1}\left(\frac{I_d}{I_q}\right) + \tan^{-1}\left(\frac{V_d}{V_q}\right)\right). \tag{16}$$

4. Design optimisation

Although wind generator drivetrain is implied in this study, the focus of the current design is on the wind generator component itself, whereby the conclusions drawn do not take into account the other associated drivetrain components. To this end, the inquiry is mainly on the performance of 12/10 PM–FSM wind generator operated under different drivetrains, with the CoE being of primary interest. The objective functions are the ratio of the average torque to PM mass and the active mass given as

$$F_1(\bar{x}) = \frac{\tau_e}{M_{PM}}, \tag{17}$$

$$F_2(\bar{x}) = M_A = M_{FeS} + M_{FeR} + M_{PM} + M_{Cu}. \tag{18}$$

The design optimisation process is subjected to the following constraint functions defined as $\mathcal{P}_{\text{out}} \geq 10$ kW, $\text{PF} \geq 0.8$, $\kappa_\delta \leq 10$ % and $\eta \geq 90$ %. To account for the different drivetrains, the mechanical speed of the generator is constrained at 30 r/min, 360 r/min and 1500 r/min which represent the LS, MS and HS drivetrains, respectively, while the airgap length (g) was kept constant at 0.7 mm for the three designs. The use of the same airgap length for the three designs may be considered unfair, especially for the LS design, but as shown in [8], in the manufacturing of a similar–sized wound–field flux switching wind generator prototype, the same airgap length is used. As a matter of fact, it is reported in [9] that for machines with exceptionally large stator outer diameter, e.g., in LS designs, an airgap ratio defined as $g/D_{out} \approx 0.001$ is preferred. Besides, for such LS designs, a small airgap is necessary to subsidize the amount of PM usage. Hence, the uniform airgap size adopted for the three designs appears to mostly favour the LS design.

The initial design is created according to the sizing method presented in [10]. Each drivetrain speed is used generate a reference design to initiate the design optimisation in respect of the design geometry. Reasonable boundary conditions are formulated for the twelve design parameters chosen as itemised in Table 1 based on a methodology formulated in [11] for wound-field FSMs. As reported in [12], the current density and current angle have been included as non–dimensional parameters so as to increase the flexibility of the optimum design considering that PM–FSMs are prone to saturation and magnetic cross–coupling effects. The flowchart outlined in Fig. 3 describes the design optimisation procedure.

The optimisation is based on a non–gradient algorithm called the Non–dominated Sorting Genetic Algorithm II (NSGA–II) [13]. NSGA–II as an adaptive search technique inspired from nature, which works on the principle of Darwin's theory of survival–of–the–fittest, and broadly referred to as evolutionary algorithm. It works with a set of solutions (population) and as the simulation (evolution) proceeds, the individuals (solution) in the population improve. On this premise, each optimisation problem is ascribed 20 individuals while 100 iterations are applied, with the tuneable crossover and mutation index set at 20 and 10, respectively.

5. Results and discussion

The simulation results of the optimisation problems executed for the three different drivetrain solutions are presented in Fig. 4, showing scatter plots of the optimal designs. It is clear that relatively less amount of PM is required to achieve the average torque requirements in the LS drivetrain, but with significant increase in the generator active mass. In reality, what is lost in terms of PM amount is traded off for an increase in the amount of copper and steel. As for the HS designs, the ratio of the torque requirement to PM mass is highest, while the smallest amount of copper and steel is used. As expected, the geared MS designs presented a tradeoff, with impressively high torque/PM densities as obtained in the LS designs and very low active mass as obtained in the HS designs.

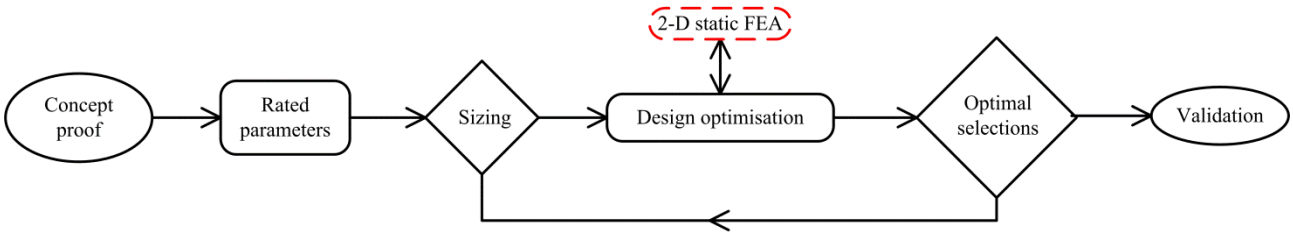

Fig. 3. PM–FSM design optimisation workflow.

Table 1
Boundary conditions defined for design parameters

Design variables	$\bar{x}$	Drivetrain					
		LS		MS		HS	
		$x^{(L)}$	$x^{(U)}$	$x^{(L)}$	$x^{(U)}$	$x^{(L)}$	$x^{(U)}$
Current angle (deg.)	α	0	90	0	90	0	90
Current density (A/mm^2)	J	1	5	1	5	1	5
Stator outer diameter (mm)	D_{out}	600	700	250	300	170	200
Stator inner diameter (mm)	D_{in}	388.5	500	162	180	120	140
Shaft diameter (mm)	D_{sh}	225	300	80	85	50	60
Stack length (mm)	l_{st}	250	500	90	180	70	140
PM length (mm)	b_{pm}	10	20	5	10	5	10
Rotor pole width (mm)	b_{pr}	20	40	10	20	7.5	15
Slot opening width (mm)	b_{sls}	12.5	25	7.5	15	5	10
Stator yoke height (mm)	h_{ys}	12.5	25	7.5	15	5	10
Rotor yoke height (mm)	h_{yr}	10	20	7.5	15	7.5	10
Rotor tooth tapering factor	t_0	0.5	1	0.5	1	0.5	1

Furthermore, the average values of the active mass for each optimal drivetrain design candidates are plotted as shown in Fig. 5. As indicated, the average active mass for the LS designs is highest compared to both the HS and MS options, given that all machines were designed for the same power levels of about 10 kW. Thus, it is perceived that the potential incorporation of gearboxes in both the MS and HS designs, while satisfying the optimum design requirements, gave rise to huge mass discrepancies of these designs compared to the LS one. But considering the generator costs, it is clearly noted that best CoE is achieved in the MS drivetrain, because unlike the HS option, its PM utilisation factor is more attractive.

To further evaluate the performance versus CoE, a representative design is benchmarked from each optimal drivetrain solution, with the baseline power requirement set within the 10 kW limit. The key performance indices for each drivetrain solution are displayed as shown in Table 2, leading to further discussions. The cost estimations are based on price quotations sourced from [14] in US dollars (USD).

As observed in Table 2, the torque–mass densities have similar trends with respect that of the torque–PM densities. Moreover, it is clearly shown that the generator costs are proportional to the torque. Hence, for the estimated total material costs, the LS generator is over 10 times the cost of the MS generator and 27 times that of the HS generator. However, between the MS and HS generators, the cost margin only differs by 250 %.

Consequently, as implied in [15], should a gearbox cost ratio of 183 % between the HS gearbox and single–stage MS gearbox be adopted, then the MS generator drivetrain costs is improved to 136 %. But with higher operation and maintenance costs accruing to the HS gearbox, the cost of the MS system is anticipated to be improved further.

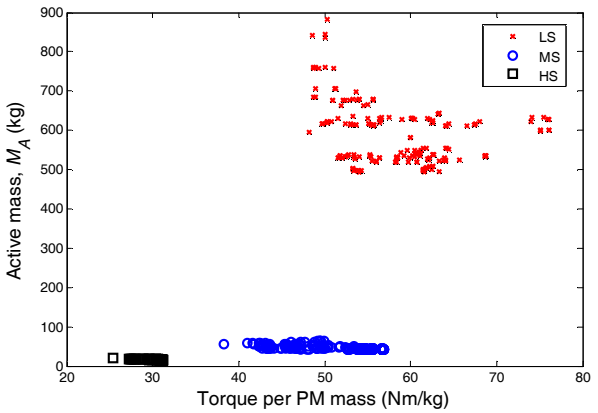

Fig. 4. Optimisation results for different PM–FSM wind generator drivetrains.

Table 2
Benchmark performance comparison of 10 kW PM–FSM wind generator drivetrains

Parameters	Units	Drivetrain		
		LS	MS	HS
Torque, τ_e	Nm	3207.17	260.47	62.33
Torque ripple, κ_δ	%	10.29	9.96	10.28
Output power, $\mathrm{P}_{\mathrm{out}}$	kW	10.24	10.03	10.04
Copper loss, P_{Cu}	kW	1.13	0.42	0.16
Core loss, P_{Core}	kW	0.02	0.09	0.26
Efficiency, η	%	90	95.12	95.95
Power factor, PF	–	0.89	0.8	0.83
Stator steel mass, M_{FeS}	kg	292.56	22.88	7.66
Rotor steel mass, M_{FeR}	kg	91.04	8.03	2.23
Copper mass, M_{Cu}	kg	58.64	6.15	2.52
PM mass, M_{PM}	kg	52.08	4.75	1.99
Active mass, M_A	kg	494.32	41.82	14.40
Torque/active mass	Nm/kg	6.49	6.23	4.33
Torque/PM mass	Nm/kg	61.58	54.83	31.32
Total material cost	USD	4625.48	421.88	169.38
Split ratio, Λ_0	–	0.63	0.57	0.53
Aspect ratio, κ_L	–	0.68	0.69	0.83
Current density, J	A/mm^2	2.673	4.999	4.999

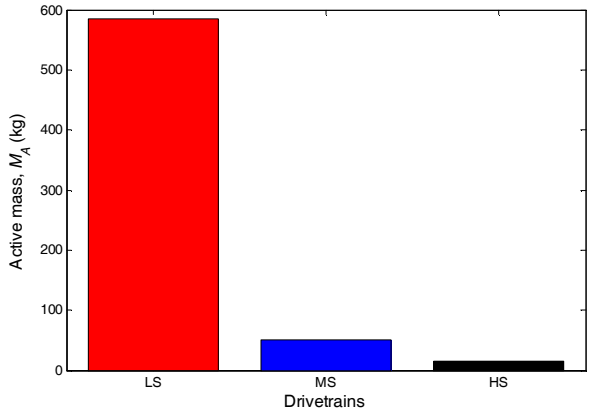

Fig. 5. Comparison of generator mass for different drivetrains.

Also, comparing power factor shows the LS design with the best outcome at 0.89; however, the prescribed power factor limit was achieved in all three drivetrains. The excellent power factor in the LS design is possible only because it incurred the lowest current density after the MDO process. To this end, the LS benchmark potentially yields the cheapest solid state converter (SSC) due to its excellent power factor compared to the rest; because, according to [16], the conduction loss of SSCs depends on power factor, which compounds their power ratings and costs. But such cost rebate might consequently be diminished considering its oversized generator, with implications for very high manufacturing and logistics costs. Or perhaps, the power factor of the LS design could have improved because of the same airgap lengths assumed on the three designs, leading to betterment of the magnetising reactance in the resulting oversized generator. To support such claims, it is reported in [9] that by decreasing the magnetic inductance of a machine, greater amount of reactive current is usually generated to the detriment of the power factor.

Looking at the torque capability of the LS design, one would expect greater torque per PM mass as compared in Table 2. Fig. 4 shows a good proportion of the evolved torque/PM mass of the LS designs in this light, while also portraying a prominent overlap with those of the MS designs.

On the other hand, the copper loss in the LS design is dominant among the three different drivetrains as observed in Table 2. Evaluation of the current values for the reported benchmarks in Table 2 resulted in 24.91 A, 12.24 A and 6.54 A for the LS, MS and HS designs, respectively. Thus, the reduction in the current density of the LS design yields corresponding decrease in the phase current, viz., $I_s^2 R_s$ loss.

The core losses in Table 2 shows the HS design has is highest among the three drivetrains, no thanks to its highest fundamental frequency. Notwithstanding, this increment is dwarfed by the copper loss recorded in the LS design, which apparently resulted in the extremely poor efficiency performance at approximately 90 %. Meanwhile, it is indicated that the efficiency in the MS and HS machines are logged in excess of 95 %. As for torque ripple, the variation among the three drivetrains is not so dramatic, while bearing in mind that each drivetrain solution satisfied the optimum design requirements.

While it may not be a conclusive task to predict

which of the generators give the best drivetrain solution, the MS design is to be acknowledged as the preferred solution because it yields the best tradeoff between CoE and performance. To reach this conclusion, the following are noteworthy:

- The torque densities (with respect to PM and total active mass) of the MS designs is as high as those observed in the LS designs, while its cost remain comparable to that of the HS designs. This should imply a reduction in the size and cost of the wind turbine tower and hub.
- The power factor is lowest for the MS generators, which due to very high current density. This means an increase in the leakage reactance, as well as the losses and cost of the SSC [17]. In any case, the higher cost implications of the LS generator and the HS gearbox should diminish their cost advantage in terms of the SSCs.
- Lastly, considering the baseline power, the MS generators yield comparable torque ripple and efficiency for the benefit of the overall drivetrain reliability and energy yield.

6. 3–D FEA Comparison

In this subsection, the design feasibility of the 2–D static FEA predictions, are compared with 3–D transient FEA solutions executed in ANSYS Maxwell© environment. The MS benchmark design from the preceding subsection is prioritised for the analyses. The magnetic flux density realised on the surface of the 3–D model is as shown in Fig. 11, while the terminal voltage waveforms calculated in 2–D and 3–D FEA are compared in Fig. 12. As can be seen, a good agreement has been obtained. The rough edges observed in the voltage waveform in 3–D FEA are likely due to less accurate meshing.

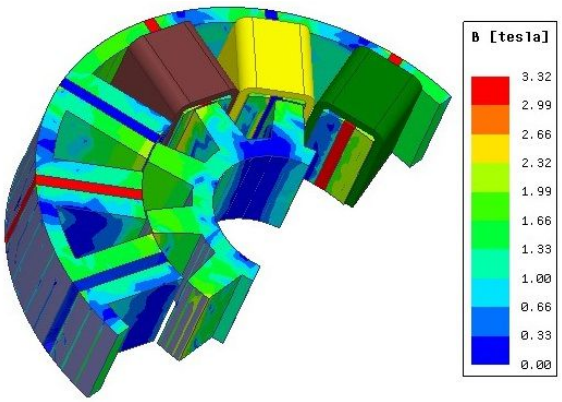

Fig. 11. 3–D FEA model showing the magnetic flux density under rated condition.

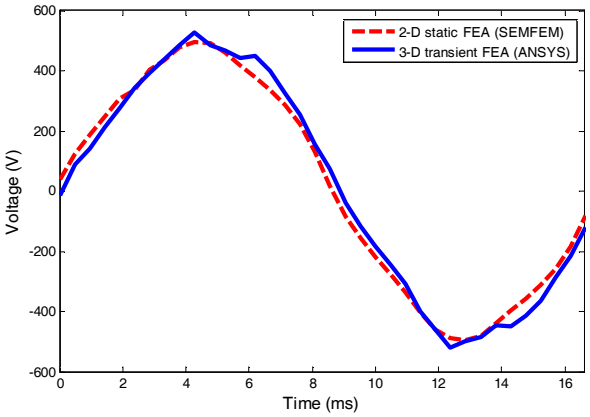

Fig. 12. Phase voltage comparison at 360 r/min.

7. Conclusion

In this study, the optimal drivetrain comparison of 12/10 PM–FSM for 10 kW wind generators has been initiated in FEA. The evaluation is on the CoE versus performance for the identified generator drivetrains—LS, MS and HS. The results show that, in terms of costs, the HS drivetrain presents the cheapest design but at the expense of the highest PM utilisation—torque per PM mass—less than 35 Nm/kg. In addition, the cost of the HS drivetrain increases to maximum due to gearbox installation and maintenance costs. On the other hand, the LS drivetrain uses the lowest amount of PM material—torque per PM mass—between 47 Nm/kg and 67 Nm/kg, but at the expense of an oversized generator. Thus, the LS active material cost is increased, to at least, 10 times the cost of the MS generator and 27 times that of the HS generator. In addition, an oversized LS generator means that the installation and logistic costs is increased. To this end, the MS design is nominated as the preferred solution because of an intrinsic trade–off in the torque/PM densities (37–57 Nm/kg) and generator costs.

Based on some optimal benchmarks from each of the three drivetrain solutions, it is observed that the huge size of the LS generator requires very high amount of copper, such that it results in high copper loss which limits the efficiency target to around 90 %, while benefiting the power factor. On the other hand, the efficiency requirements of the MS and HS designs are both well–exceeded, i.e., beyond 95 %, both with respectable power factor.

In summary, the study focused on the optimal wind generator drivetrain comparison of the 12/10 PM–FSM, showing the MS design as the preferred solution among the three drivetrains. However, a firm conclusion cannot be reached because only the electromagnetic design and performance of the generators are fully addressed in the study, while other

drivetrains components such as gearboxes and SSCs were only considered as estimates.

References

1. E. de Vries, *ABB shifts focus to medium speed drive systems*, WINDPOWER Monthly, 4 September 2012.
2. S. Schmidt and A. Vath, "Comparison of existing medium–speed drive train concepts with a differential gearbox approach," *European Wind Energy Association*, Copenhagen, pp. 179–186, April 2012.
3. W. Cao, Y. Xie and Z. Tan, *Wind turbine generator technologies*, InTech, 2012.
4. D–J Bang, H.P. Under, G. Shrestha and J. Ferreira, "Promising direct–drive generator system for large wind turbines," *Wind Power to the Grid Seminar*, EPE–WECS, 2008.
5. S. E. Rauch and L. J. Johnson, "Design principles of flux–switching alternators," *AIEE Trans.*, 74(III), pp. 1261–1268, 1955.
6. M. Cheng, W. Hua, J. Zhang, and W. Zhao, "Overview of stator–permanent magnet brushless machines," *IEEE Transactions on Industrial Electronics*, 58(11), pp. 5087–5101, 2011.
7. SEMFEM online documentation. [Online]. Available: www0.sun.ac.za/semfem/index.html
8. U.B. Akuru and M.J. Kamper, "Intriguing Behavioural Characteristics of Rare-Earth-Free Flux Switching Wind Generators at Small- and Large-Scale Power Levels," IEEE Transactions on Industry Applications, 54(6), pp. 5772-5782, Nov/Dec 2018.
9. J. Pyrhönen, T. Jokinen and V. Hrabovcova, *Design of Rotating Electrical Machines*, 5th ed., John Wiley & Sons, Ltd: UK, 2008.
10. W. Hua, C. Ming, Z. Q. Zhu and D. Howe, "Design of flux–switching permanent magnet machine considering the limitation of inverter and flux–weakening capability," *Conference Record of the IEEE Industry Applications Conference, 41st IAS Annual Meeting.*, vol.5, pp.2403–2410, 8–12 Oct. 2006.
11. U. B. Akuru and M. J. Kamper, "Formulation and multi-objective design optimisation of wound-field flux switching machines for wind energy drives," *IEEE Transactions on Industrial Electronics*, 65(2), pp. 1828-1836, Feb. 2018.
12. E. Ilhan, M. F. J. Kremers, E. T. Motoasca, J. J. H. Paulides and E. A. Lomonova, "Sensitivity analysis for phase inductances in Flux–Switching PM machines," *XXth International Conference on Electrical Machines*, Marseille, pp. 763–768, 2012.
13. K. Deb, A. Pratap, S. Agarwal and T. Meyarivan, "A fast and elitist multiobjective genetic algorithm: NSGA–II," *IEEE Transactions on Evolutionary Computation*, 6(2), pp. 182–197, Apr. 2002.
14. A. Fasolo, L. Alberti and N. Bianchi, "Performance comparison between switching–flux and IPM machines with rare–earth and ferrite PMs," *IEEE Transactions on Industry Applications*, 50(6), pp. 3708–3716, Nov.–Dec. 2014.
15. H. Polinder, F. F. A. van der Pijl, G. J. de Vilder and P. J. Tavner, "Comparison of direct–drive and geared generator concepts for wind turbines," *IEEE Transactions on Energy Conversion*, 21(3), pp. 725–733, Sept. 2006.
16. E. B. Sulaiman, T. Kosaka and N. Matsui, "Design study and experimental analysis of wound field flux switching motor for HEV applications," *XXth International Conference on Electrical Machines* (ICEM), pp.1269–1275, 2–5 Sept. 2012.
17. I. Boldea, L. Tutelea and F. Blaabjerg, "High power wind generator designs with less or no PMs: An overview," *17th International Conference on Electrical Machines and Systems* (ICEMS), pp.1–14, 22–25 Oct. 2014.